

Canonical Trajectories and Critical Coupling of the Bose-Hubbard Hamiltonian in a Harmonic Trap

G.G. Batrouni¹, H. R. Krishnamurthy^{2,3}, K. W. Mahmud², V.G. Rousseau⁴, and R.T. Scalettar²

¹*INLN, Université de Nice-Sophia Antipolis, CNRS; 1361 route des Lucioles, 06560 Valbonne, France*

²*Physics Department, University of California, Davis, California 95616, USA*

³*Centre for Condensed Matter Theory, Department of Physics, Indian Institute of Science, Bangalore 560012, India and*

⁴*Lorentz Institute, Leiden University, P. O. Box 9506, 2300 RA Leiden, The Netherlands*

Quantum Monte Carlo (QMC) simulations and the Local Density Approximation (LDA) are used to map the constant particle number (canonical) trajectories of the Bose Hubbard Hamiltonian confined in a harmonic trap onto the $(\mu/U, t/U)$ phase diagram of the uniform system. Generically, these curves do not intercept the tips of the Mott insulator (MI) lobes of the uniform system. This observation necessitates a clarification of the appropriate comparison between critical couplings obtained in experiments on trapped systems with those obtained in QMC simulations. The density profiles and visibility are also obtained along these trajectories. Density profiles from QMC in the confined case are compared with LDA results.

PACS numbers: 03.75.Kk, 03.75.Lm, 03.75.Hh, 05.30.Jp

The bosonic Hubbard model was first introduced¹ in the context of disordered superconductors where the superfluidity of preformed Cooper pairs competes with Mott insulator and Bose glass phases. Considerable numerical work followed the original analytic treatment. When there is no disorder, Quantum Monte Carlo (QMC) studies^{2,3} obtained quantitative values for the critical coupling of the superfluid-Mott insulator (SF-MI) transition at commensurate filling in one dimension, which were in good quantitative agreement with series expansion⁴ and density matrix renormalization group calculations^{5,6}. The critical point is now known in $d = 2$ to a very high accuracy⁷.

Over the last decade, it became clear that trapped ultra-cold atoms provide an alternate, and more controllable, experimental realization of the bosonic Hubbard model⁸. Indeed, the possibility of a quantitative comparison of theoretical and experimental values for the critical point has been suggested. A recent experimental paper⁹ has offered the first such benchmark in $d = 2$.

However, a significant obstacle exists for such a direct comparison: The confining potential produces spatial inhomogeneities and a coexistence of SF and MI phases¹⁰. This naturally leads to the question as to what “critical coupling” is being accessed in the experiments. Is it the coupling at which “Mott shoulders” begin to develop about a SF core? Or is it the coupling at which a Mott region pervades the entire central region of the trap? In this paper, we provide a detailed quantitative analysis of this issue. Specifically, using the Local Density Approximation (LDA) and QMC simulations, we study, for fixed particle numbers, the evolution of the density profiles of the trapped system as a function of the interaction strength and map those “canonical trajectories” onto the phase diagram of the uniform system. We also show data for the visibility^{11,12}. These measurements allow us to connect the critical points obtained in QMC with those that can be seen in experiment.

The QMC results presented here were obtained using two different algorithms. In the first¹⁵, the imaginary time β is discretized leading to a path integral for the partition function on a rigid space-imaginary time grid with local world line updates. In the second^{16,17,18}, imaginary time is continuous and there are no Trotter errors associated with discretization. Bosonic world-line updates can be non-local, and, as a consequence, the Green’s function can be measured at all separations. The two algorithms give consistent results for all physical quantities calculated such as the density profiles and superfluid density.

The one dimensional bosonic Hubbard Hamiltonian is,

$$H = -t \sum_i \left(a_i^\dagger a_{i+1} + a_{i+1}^\dagger a_i \right) - \mu \sum_i n_i + V_T \sum_i x_i^2 n_i + \frac{U}{2} \sum_i n_i (n_i - 1). \quad (1)$$

Here $i = 1, 2, \dots, L$ where L is the number of sites and $x_i = a|i - L/2|$ is the coordinate of the i th site as measured from the center of the system. We choose the lattice constant $a = 1$. The hopping parameter, t , sets the energy scale; in what follows we set $t = 1$, i.e., all energies are measured in units of t . $n_i = a_i^\dagger a_i$ is the number operator, and $[a_i, a_j^\dagger] = \delta_{ij}$ are bosonic creation and destruction operators. V_T is the curvature of the trap, and the repulsive contact interaction is given by U . The chemical potential, μ , controls the average number of particles.

The bosonic-Hubbard Hamiltonian can also be simulated in the canonical ensemble at fixed particle number N_b . Indeed this is essential in order to make contact with experiments. In the homogeneous case, $V_T = 0$, the phase diagram is a function of the density, N_b/L^d , and the interaction U/t where d is the dimensionality of the system. It was emphasized recently¹⁴ that a similar lattice size independent formulation can be made in the confined case by using a rescaled length $\xi_i \equiv x_i/\xi$ with

$\xi = \sqrt{t/V_T}$. Then, density profiles and the resulting phase diagram depend on N_b and V_T only via the combination $\tilde{\rho} = N_b/\xi^d$, called the ‘‘characteristic density’’.

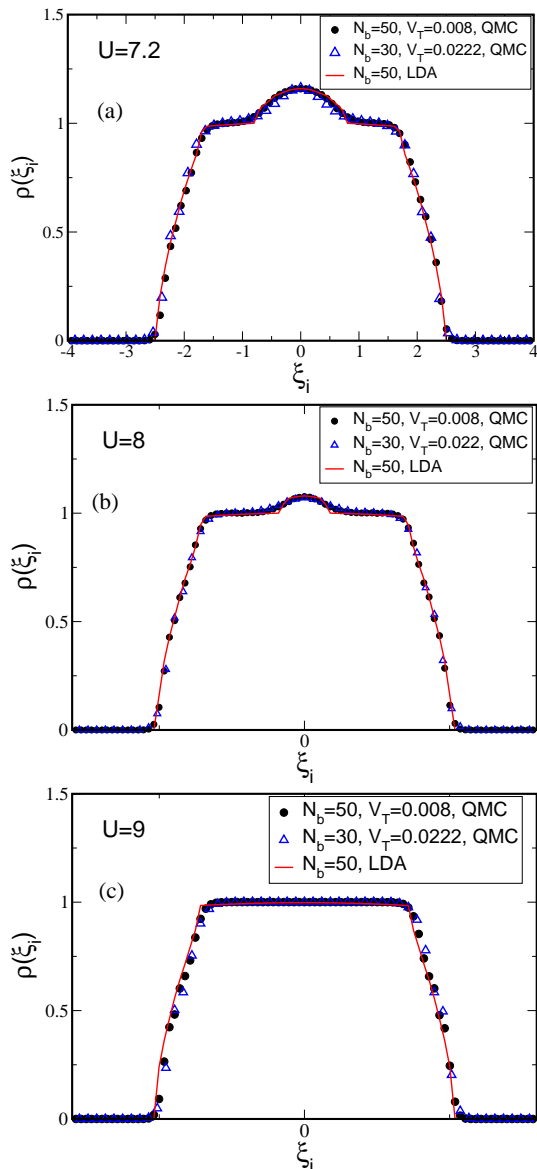


FIG. 1: (Color online) Density profiles *vs* the rescaled position, ξ_i , in $1d$. The solid lines are obtained using QMC for the uniform system combined with the LDA to include the trap. The symbols are the results of QMC done directly on the confined system. The characteristic density $\tilde{\rho} = 4.47$ and $U = 7.2, 8.0, 9.0$. We also show, in the three panels, profiles for two different particle numbers, $N_b = 50, 30$ but with the same $\tilde{\rho} = 4.47$.

One simple way to understand the role of the characteristic density and to infer the properties of the trapped system is the Local Density Approximation (LDA)¹³ in which the density at a particular location x_i in the trapped system is assumed to be given by the density of a uniform system with chemical potential equal to the ‘‘local chemical potential’’ $\mu_i \equiv \mu - V_T x_i^2$ at that location.

In other words, for a trapped $1d$ system,

$$\rho(x_i) \equiv \langle n_i \rangle_{V_T} = \rho_{1d}^0(\mu_i; U), \quad (2)$$

where $\rho_{1d}^0(\mu; U) \equiv \langle n_i \rangle_{V_T=0}$ is the density for the $1d$ bosonic Hubbard model in the homogeneous case. For a given desired N_b , the requisite chemical potential μ in the presence of the trap, which is also the *local* chemical potential at the center of the trap, is determined by the condition,

$$N_b = \sum_i \langle n_i \rangle_{V_T} = \sum_i \rho_{1d}^0(\mu - V_T x_i^2; U), \quad (3)$$

and is therefore implicitly a function of N_b, U and V_T . In principle, one can use $\rho_{1d}^0(\mu; U)$ as determined by QMC in the uniform case, together with Eq. (3) to determine μ . Within the LDA the density profile $\rho(x_i)$ is then completely determined, and can be compared with results obtained directly from simulations with a trap potential to determine the accuracy of the LDA, as discussed below. Furthermore, Eq. (3) provides a useful guide to understanding the trajectories in the (μ, U) plane that are traversed in experimental investigations such as in Ref. 9, since they are typically done at fixed N_b and varying t by varying the depth of the optical potential (which, however, also changes the trap potential).

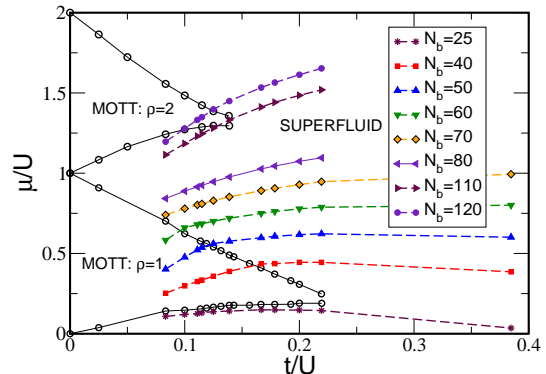


FIG. 2: (Color online) Canonical (constant particle number) flows in the $(\mu/U, t/U)$ plane at fixed $V_T = 0.008$. Characteristic densities vary from $\tilde{\rho} = 2.24$ for $N_b = 25$ (lowest curve) to $\tilde{\rho} = 10.73$ for $N_b = 120$ (highest curve).

Better insight into the nature of such *canonical* (constant N_b) trajectories is obtained by approximating the sum in Eq. (3) as an integral. This should be a reasonable approximation when the local chemical potential changes slowly from site to site, i.e. in the same regime where LDA is expected to be valid. In the one dimensional case¹⁹ one has,

$$N_b = 2 \int_0^\infty dx \rho_{1d}^0(\mu - V_T x^2; U). \quad (4)$$

Changing the integration variable to $\mu_x \equiv \mu - V_T x^2$, this equation can be rewritten as¹⁹,

$$N_b \sqrt{V_T} \equiv \tilde{\rho} = \int_{-\infty}^\mu \frac{d\mu_x \rho_{1d}^0(\mu_x; U)}{\sqrt{\mu - \mu_x}} \equiv I_1(\mu; U). \quad (5)$$

I_1 is entirely determined from the solution of the homogeneous problem. The chemical potential in the presence of the trap, μ , is determined by inverting Eq. (5). Note the natural appearance of the characteristic density $\tilde{\rho}$ on the left side of Eq. (5). Clearly, μ , and hence the density profile expressed as a function of x/ξ , depend only on $\tilde{\rho}$ and not on N_b and V_T separately. Needless to say, I_1 can also be computed directly by evaluating the sum in Eq. (3) using the simulation results for ρ_{1d}^0 .

Thermodynamic stability implies that ρ_{1d}^0 , and hence $I_1(\mu; U)$, are monotonically increasing functions²⁰ of μ . For $\tilde{\rho} < I_1(\mu_1^-(U); U) \equiv \tilde{\rho}_1^-(U)$, μ , and hence μ_i , are less than $\mu_1^-(U)$, the chemical potential at which the first Mott lobe is reached from below. Therefore $\rho(x_i) < 1$, and all sites are sampling the SF region in the phase diagram below the first Mott lobe (if $U > U_c$).

The density profile is very different when U , V_T and N_b are such that $\tilde{\rho}$ is larger than $\tilde{\rho}_1^-(U)$. Then $\mu > \mu_1^-(U)$ and therefore a flat Mott plateau with $\rho(x_i) = 1$ appears in the central region of the system, extending over sites i for which $\mu_i \geq \mu_1^-(U)$. For sites outside this plateau, $\rho(x_i) < 1$ and the system is locally in the SF phase.

If the trap potential is increased so as to squeeze the particles towards the center of the cell (or if N_b is increased), $\tilde{\rho}$ and μ increase. For $\tilde{\rho} > I_1(\mu_1^+(U); U) \equiv \tilde{\rho}_1^+(U)$, one has $\mu > \mu_1^+(U)$, the chemical potential at which the first Mott lobe is reached from above. In this case the central sites of the system are in the superfluid region above the Mott lobe, with $\rho(x_i) > 1$, surrounded by MI shoulders where $\rho(x_i) = 1$, in turn surrounded by SF regions as the edges of the system are reached (Fig. 1(a)).

In the regime $\tilde{\rho}_1^-(U) < \tilde{\rho} < \tilde{\rho}_1^+(U)$, as is easily verified from Eq. (5), μ is determined by the equation,

$$\mu - \mu_1^-(U) = [\tilde{\rho} - \tilde{\rho}_1^-(U)]^2/4. \quad (6)$$

Hence the two threshold values of $\tilde{\rho}$ in the presence of the trap and the threshold chemical potentials for the Mott transition in the homogeneous case are related via,

$$\mu_1^+(U) - \mu_1^-(U) = [\tilde{\rho}_1^+(U) - \tilde{\rho}_1^-(U)]^2/4. \quad (7)$$

For larger values of $\tilde{\rho}$ in large systems with a small V_T , one can access transitions involving the higher Mott lobes¹⁰.

In Fig. 1 we compare the density profiles obtained from direct QMC simulations of the trapped system with those inferred from the LDA and QMC simulations of the uniform system. The LDA generally provides an accurate description of the density profiles except at those locations in the trap where a changeover from superfluid to Mott insulator region is occurring. This is clear in Fig. 1 where as one goes from SF to MI regions, the transition is much sharper for the LDA curves. This, of course, is a vestige of the true quantum phase transition present in the unconfined system on which the LDA method is based. Figure 1 shows profiles for two different pairs of (N_b, V_T) which have the same characteristic density.

They are seen to coincide almost perfectly, validating the use of ξ_i and $\tilde{\rho}$ to describe the physics in a scale-independent way.

Figure 2 shows the canonical trajectories corresponding to $\mu(\tilde{\rho}, U)$ for fixed $\tilde{\rho}$, obtained from Eq. (3), superimposed on the phase diagram of the uniform system. Each trajectory is at constant N_b and, therefore, constant $\tilde{\rho}$ when V_T is fixed, and shows where the trapped system sits in the phase diagram of the uniform system when the LDA is used in combination with QMC. For example, for the confined system values $N_b = 50$, $V_T = 0.008$ and $U = 9.0$, $\mu(\tilde{\rho}, U)$, lies well within the $\rho = 1$ Mott lobe and the system should be a Mott insulator according to this mapping. Figure 1(c) shows the true density profile obtained with QMC directly with a trap and we see that, indeed, the confined system is a MI, except for the edges which always have $\rho(x_i) < 1$. On the other hand, staying on the same trajectory, $N_b = 50$, but with $U = 7.2$, the $\mu(\tilde{\rho}, U)$ lies in the SF phase above the Mott lobe leading us to predict the central region of the trapped system to be SF with $\rho(x_i) > 1$, as indeed confirmed by Fig. 1(a). A second example of this evolution, for $N_b = 110$, which just clips the top of the $\rho = 2$ Mott lobe, is given in Fig. 3, with similar conclusions. Notice that as U increases, if a trajectory enters, say, the $\rho = 2$ Mott lobe, it will leave it eventually upon further increases in U . Such a trajectory will eventually enter the $\rho = 1$ Mott lobe which it can never leave.

It is important to note that different trajectories intersect the Mott lobes at different $(\mu/U, t/U)$ points and in general *not* at the tip. Thus, Fig. 2 emphasizes the central point of this paper, namely that *both* the particle number and confining potential need to be considered together in determining the ‘critical point’ of the trapped boson Hubbard Hamiltonian. In particular, in order to access U_c in an experiment, the characteristic density also has to be tuned to its appropriate critical value. In the case of a 1-d trapped system we are considering in this paper, $\tilde{\rho}_c \simeq 2.7$.

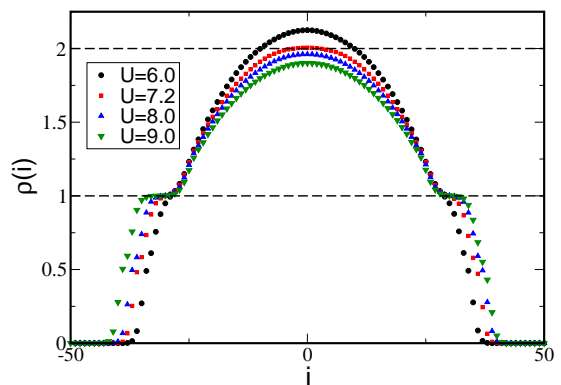


FIG. 3: (Color online) Density profiles along the $N_b = 110$ ($\tilde{\rho} = 9.84$) trajectory. This value just clips the tip of the uniform system $\rho = 2$ lobe, as seen in Fig. 2. The dashed lines are to draw attention to the $\rho = 1, 2$ values where the MI develops.

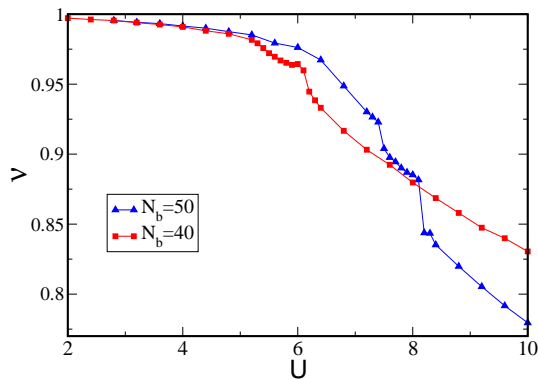


FIG. 4: (Color online) The visibility along the $N_b = 40$ and $N_b = 50$ trajectories (corresponding to $\tilde{\rho} = 3.58$ and 4.47 with $V_T = 0.008$). For $N_b = 50$ the kink at $U = 7.5$ is associated with the presence of well-formed Mott shoulders. The second kink at $U = 8.2$ corresponds to the formation of a full Mott phase throughout the center of the trap ($V_T = 0.008$).

Our understanding of the relation between the density profiles and the “flow diagram” of canonical trajectories is made complete by examining the visibility \mathcal{V} , which is known to be a sensitive measure of the behavior of the density profiles^{11,12}. For $N_b = 50$ ($\tilde{\rho} = 4.47$), \mathcal{V} has two kinks at $U = 7.5$ and $U = 8.2$ which indicate respectively the appearance of well-formed Mott shoulders surrounding a SF interior and then the total disappearance of superfluidity at the trap center and the establishment of MI throughout (Fig. 4). It is seen from Fig. 2 that the second, larger, of these two values corresponds very well to the coupling where the $N_b = 50$ trajectory enters the

uniform system Mott lobe.

In summary, in this paper we have shown that for fixed particle number, the “critical coupling” associated with destruction of superfluidity and onset of Mott behavior depends on the characteristic density $\tilde{\rho}$. In fact, this observation is also implicit in the “state diagram” of [10] in which the boundaries between phases at fixed V_T were shown to depend on N_b . Using the local density approximation we explicitly constructed the trajectories in the $(\mu/U, t/U)$ plane which correspond to constant $\tilde{\rho}$, and quantified their points of entry into the Mott lobe of the uniform system. This construction should allow experimentalists to predict where, on the phase diagram of the uniform system, their trapped system will be. The behavior of the visibility confirmed that the uniform Mott lobe is entered when the center of the density profiles is in the Mott phase.

We have focused here on $d = 1$. However, the basic qualitative point we wish to emphasize is valid in any dimension: a careful consideration of the confining potential in addition to the number of particles is essential for a meaningful comparison of the critical couplings obtained in experiments with those of the homogeneous system.

Supported under ARO Award W911NF0710576 with funds from the DARPA OLE Program. G.G.B. supported in part by the CNRS (France) PICS 18796. We acknowledge very useful conversations with M. Rigol, J.K. Freericks and B.L. Polisar. We thank L. Pollet for commenting on equilibration problems in an early version of Fig.1b.

¹ M.P.A. Fisher *et al.*, Phys. Rev. **B40**, 546 (1989).

² G.G. Batrouni, R.T. Scalettar, and G.T. Zimanyi, Phys. Rev. Lett. **65**, 1765 (1990).

³ N.V. Prokof'ev and B.V. Svistunov, Phys. Rev. Lett. **80**, 4355 (1998).

⁴ J.K. Freericks and H. Monien, Phys. Rev. **B53**, 2691 (1996).

⁵ T.D. Kühner and H. Monien, Phys. Rev. **B58**, R14741 (1998).

⁶ T.D. Kühner, S.R. White, and H. Monien, Phys. Rev. **B61**, 12474 (2000).

⁷ B. Capogrosso-Sansone *et al.*, cond-mat/0710.2703.

⁸ D. Jaksch *et al.*, Phys. Rev. Lett. **81**, 3108 (1998).

⁹ I. Spielman and T. Porto, private communication.

¹⁰ G.G. Batrouni *et al.*, Phys. Rev. Lett. **89**, 117203 (2002).

¹¹ F. Gerbier *et al.*, Phys. Rev. Lett. **95**, 050404 (2005), and cond-mat/0507087.

¹² P. Sengupta *et al.*, Phys. Rev. Lett. **95**, 220402 (2005).

¹³ S. Bergkvist, P. Henelius, and A. Rosengren, Phys. Rev. **A70** 053601 (2004).

¹⁴ M. Rigol and A. Muramatsu, Phys. Rev. **A69**, 053612 (2004); Opt. Commun. **243**, 33 (2004)

¹⁵ J.E. Hirsch *et al.*, Phys. Rev. **B26**, 5033 (1982).

¹⁶ B.B. Beard and U.J. Wiese, Phys. Rev. Lett. **77**, 5130 (1996).

¹⁷ N.V. Prokof'ev, B.V. Svistunov, and I.S. Tupitsyn, J. Expt. and Theor. Phys. **64**, 911 (1996).

¹⁸ S.M.A. Rombouts, K. Van Houcke, and L. Pollet, Phys. Rev. Lett. **96**, 180603 (2006).

¹⁹ Similar considerations hold in higher dimensions, with appropriate alterations. In $2d$ one has,

$$N_b = 2\pi \int_0^\infty r dr \rho_{2d}^0(\mu - V_T r^2; U);$$

$$N_b V_T \equiv \tilde{\rho} = \pi \int_{-\infty}^\mu d\mu_r \rho_{2d}^0(\mu_r; U) \equiv I_2(\mu; U).$$

Similarly, in $3d$,

$$N_b = 4\pi \int_0^\infty r^2 dr \rho_{3d}^0(\mu - V_T r^2; U);$$

$$N_b V_T^{3/2} \equiv \tilde{\rho} = 2\pi \int_{-\infty}^\mu d\mu_r \rho_{3d}^0(\mu_r; U) \sqrt{\mu - \mu_r} \equiv I_3(\mu; U).$$

²⁰ Although $\rho(\mu)$ is monotonic, it of course exhibits interesting features like a Mott plateau where ρ is constant for a range of μ , for U sufficiently large, and a diverging derivative $\kappa = \frac{\partial \rho}{\partial \mu}$ as the Mott plateaus are approached^{1,2}.